ISSN 1392–1320 MATERIALS SCIENCE (MEDŽIAGOTYRA). Vol. XX, No. X. 2023

Investigation of Plasmonic Properties of a Rhodium Nanoshell Based Optical Nanomaterial

Quan JIANG [1], Yue ZHANG [1], Tao XIONG [1, 2], Dandan DONG [1], Wei WANG [1], Cheng SUN [1, 2] *

[1] *College of Physical Science and Technology, Dalian University, No. 10 Xuefu Avenue, Economic Technological Development Zone, Dalian, Liaoning Province, 116622, China*
[2] *Liaoning Engineering Laboratory of Optoelectronic Information Technology, No. 10 Xuefu Avenue, Economic Technological Development Zone, Dalian, Liaoning Province, 116622, China*

crossref http://dx.doi.org/10.5755/j02.ms.31413

Received 18 May 2022; accepted 30 June 2022

In noble metals, surface plasmons may be induced by incident light, resulting in good plasmonic properties that can be widely utilized. In this work, an optical nanomaterial based on a spherical nanoshell structure consisting of rhodium and dielectric is proposed. The scattering efficiency and electric field are calculated via the finite difference time domain method, by respectively varying the nanoparticle radius, the thickness of the nanoshell, as well as the dielectric material of the core. The results show that under certain conditions in the ultraviolet regime, two plasmonic resonance peaks are observed in the scattering spectrum, correlating to two different electromagnetic modes. It is also demonstrated that the resonance wavelengths and the peak intensities of the rhodium based optical nanomaterial can effectively be tuned by changing the structural parameters. The proposed rhodium-based nanomaterial may be useful in applications of optical devices in the ultraviolet regime.
Keywords: rhodium nanoshell, ultraviolet, finite difference time domain, scattering efficiency.

1. INTRODUCTION

In noble metal based optical nanomaterials, Surface Plasmons (SPs) with specific energy and frequency may be excited under the irradiation of incident light [1, 2, 3]. The induced optical properties and corresponding electromagnetic fields can widely be applied in photonics, electronics, field enhancements, and catalysis, etc. [4, 5, 6, 7]. Nanomaterials with certain symmetries have been demonstrated to exhibit great plasmonic properties [8]. Among the symmetries, core-shell structures have advantages including the simple preparation and a wide tuning range of plasmonic resonance wavelength [9]. For example, the effects of light polarization and geometrical parameters on the plasmonic resonance of multilayer nanoshells were reported [10]. The dimension dependent optical properties of spherical core-shell structures, which were composed of ZnO@Ag nanoparticles embedded in a dielectric matrix, were investigated; two sets of formants were found in different wavelength regions [11]. In addition, the plasmonic resonance wavelengths of the core-shell nanospheres based on silver and graphene were discussed [12, 13]. Recently, the extinction spectra of silver nanoshells with different environmental media were also addressed [14].

At present, the noble metals that have been extensively studied are mainly silver and gold, whose resonance wavelengths appear in the visible light regime [15]. In addition to the visible spectrum, the ultraviolet (UV) range also has a variety of practical applications due to its shorter wavelength and greater energy. Therefore, it is also significant to study noble metals that possess good plasmonic properties in the UV regime. Studies have shown that aluminium is a promising candidate for plasmonics in the UV range. UV-absorbing and high-brightness dielectric films were deposited on aluminium nanoarrays, and photoluminescence enhancement of the films under UV laser excitation was observed, and the study showed that periodic arrays of aluminium nanopillars are useful for controlling UV light [16]. However, aluminium presents a high oxidation tendency that has a critical effect on its plasmonic performance. It has been found that rhodium has a good plasmonic response in the UV spectrum in terms of the field-enhancement factor and low tendency of oxidation [17]. For instance, it was shown that the plasmonic resonance can effectively be adjusted in UV region, by changing the size and shape of rhodium nanomaterials [18]. The optical properties of rhodium-based nanostructures and their applications in catalysis were also reported [17, 19]. Theoretically, based on the SPs enhancement effect of rhodium nanoparticles, the potential use in UV photocatalysis was addressed [20]. In addition, the SPs characteristics and the applications in biochemical sensing was also reported on several rhodium-related nanoparticles [21].

In this work, an optical nanomaterial, which consists of a rhodium shell and a dielectric core, was proposed. The scattering efficiency and the electric field distribution were probed in the UV regime. Two plasmonic resonances, associated with different electromagnetic modes, were addressed. The structure has good tunability, and the plasmonic wavelength in the UV region can be tuned by changing the size of the nanoshell; similar effects were also addressed [22]. Given the advantage of the low tendency of

*Corresponding author. Tel.: +86-411-87402712; fax: +86-411-87402712. E-mail address: *suncheng@dlu.edu.cn* (C. Sun)

oxidation and the fact that several rhodium-based nanostructures have been successfully synthesized [17], the rhodium nanoshell structure proposed in this work may be experimentally produced and practically utilized.

2. STRUCTURE AND METHOD

The spherical nanoshell structure based nanomaterial consisting of rhodium and dielectric is shown in Fig. 1. In this work, the radius of the core was indicated in *r*, and the dielectric material was SiO_2 (n = 1.4), Si_3N_4 (n = 2.0), and TiO_2 (n = 2.9), respectively. Note that although there is a dispersion for the dielectric materials (within 10 %), the approximation that a non-dispersive refractive index was used in the simulations for simplicity. The nanoshell was composed of rhodium, and its radius is labeled as *R*.

Numerical simulations were performed by using the finite difference time domain (FDTD) method [23]. An *x*-polarized plane-wave light was incident along the *z*-axis, in the wavelength range of 100 – 800 nm. To avoid the possible artifacts that might be induced by the simulation method, the mesh size was always kept smaller than 1/10 of the shortest wavelength studied in the simulation region of non plasmon-carrying media. In the simulation, perfect matching layer (PML) boundary conditions were used in all directions. The optical constants of rhodium were from Palik's experimental data [24].

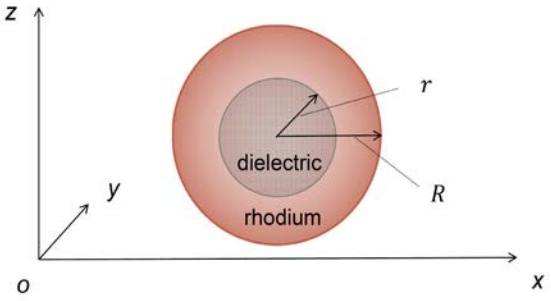

Fig. 1. The structure of the spherical nanoshell consisting of rhodium and dielectric. The radius of the dielectric core is labeled *r*, and the radius of the rhodium nanoshell is indicated in *R*

Note that no error estimates are given in this work, since the results are all calculated by using simulations, and they need to be used with caution, especially when compared with experimental data.

3. RESULTS AND DISCUSSION

3.1. Fixed radius of the dielectric core

First, the effects of the radius of the rhodium nanoshell were studied. Based on the configuration shown in Fig. 1, the scattering efficiency was calculated by the following relationship:

$$\text{Scattering Efficiency} = C_{scat}/S., \quad (1)$$

where C_{scat} is the scattering cross section of the nanostructure that was simulated by using a Total-field scattered-field (TFSF) source [23], and *S* is the projected cross-sectional area of the spherical nanoshell in the x-y plane. The scattering efficiency was calculated with a fixed value of the radius of the dielectric core (i.e., r = 10 nm), and the results are presented in Fig. 2. In the simulations, SiO_2, Si_3N_4, and TiO_2 was respectively used as the dielectric material of the core. The nanoshell's radius was varied from R = 15 to 35 nm. Note that only the scattering efficiency was used to probe the system in this work, without considering the effects that may be caused by the absorption of the dielectric core; the scheme employed in this work is a simplified model, which needs to be used with caution.

In Fig. 2 a, when the radius is large ($R \geq 25$ nm), one pronounced peak is observed in the scattering efficiency curve, within the UV range of 220 – 250 nm; the peak is labeled as L in this work, for simplicity. This peak is a clear manifestation of the plasmonic resonance that occurs in the rhodium nanoshell structure. As *R* is decreased from 35 to 25 nm, the resonance wavelength of peak L is blueshifted; similar size-dependent effects were also reported in noble metals of silver and gold in previous work [25]. Referring to Fig. 2 a again, for the small radius of R = 15 nm, in addition to peak L, another peak at about 120 nm is also witnessed in the scattering spectrum. Note that the peak at the shorter UV wavelength is indicated in S, for simplicity.

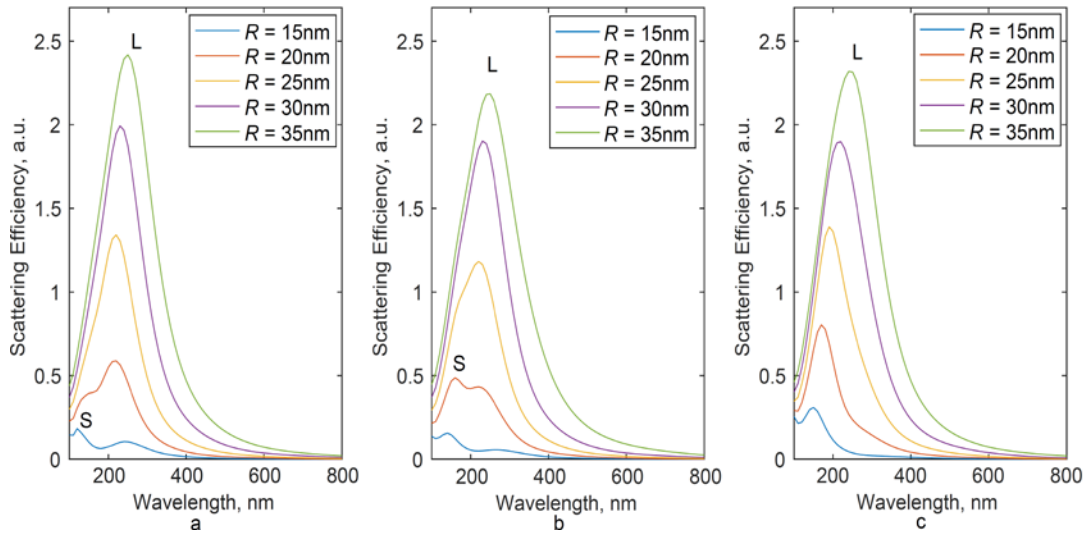

Fig. 2. Scattering efficiency as a function of incident light's wavelength. The dielectric material in the core was a – SiO_2; b – Si_3N_4; c – TiO_2. The radius of the core was fixed to be r = 10 nm

This observation reveals that when the shell radius is small, the thickness of the rhodium nanoshell is also small ($R - r$ = 5 nm), the plasmonic coupling effect between the rhodium and the dielectric core becomes more substantial, resulting in two distinguishable resonance peaks in the UV regime. These peaks may be attributed to two different plasmonic resonance modes, which will be addressed below, with the aid of electric field distributions of the nanostructure. Regarding the results for Si_3N_4 shown in Fig. 2 b, as with SiO_2, when the radius is large enough only one resonance peak (denoted L) appears. As the radius is reduced from 35 to 25 nm, the resonance wavelength is also blueshifted in the UV region from 230 to 220 nm. Once the radius is as small as 20 nm, a second peak (labeled S) at the shorter wavelength at about 160 nm becomes obvious. With further reducing the radius, the intensity of peak S overtakes that of peak L, indicating that this resonance mode becomes dominant.

It is shown in Fig. 2 c that TiO_2 is different from SiO_2 and Si_3N_4, and there appears only one peak in the UV range of 150 – 240 nm for all the radii studied. This infers that the two resonances may overlap in the wavelength domain and become not separable. In order to distinguish these two resonance modes in each condition, electric field distributions may provide more details about the underlying physics. Therefore, the computed fields are plotted in Fig. 3 – Fig. 5, corresponding to the dielectric core of SiO_2, Si_3N_4, and TiO_2, respectively.

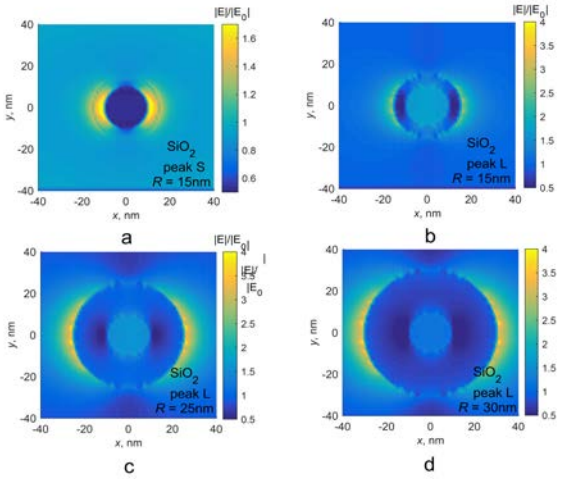

Fig. 3. Electric field distribution in the *x-y* plane for the case shown in Fig. 2 a. The nanoshell radius R: a, b – 15 nm; c – 25 nm; d – 30 nm. The wavelength correlates to a peak S, and b, c, d peak L. Note that the maximum intensity of the color bar is not the same

By comparing Fig. 3 a and b, it is clear that peaks S and L have different electric field distributions, correlating to two plasmonic modes. This verifies the previous observation in the scattering curves shown in Fig. 2 a, which reveals that the rhodium nanoshell may undergo two different plasmonic resonances once the shell radius is small. By examining Fig. 3 b – d, the similarity in the field distributions clearly demonstrates that the resonance at the longer wavelength is indeed attributed to peak L, which verifies again the above assignments of the resonance peaks, as indicated in Fig. 2 a.

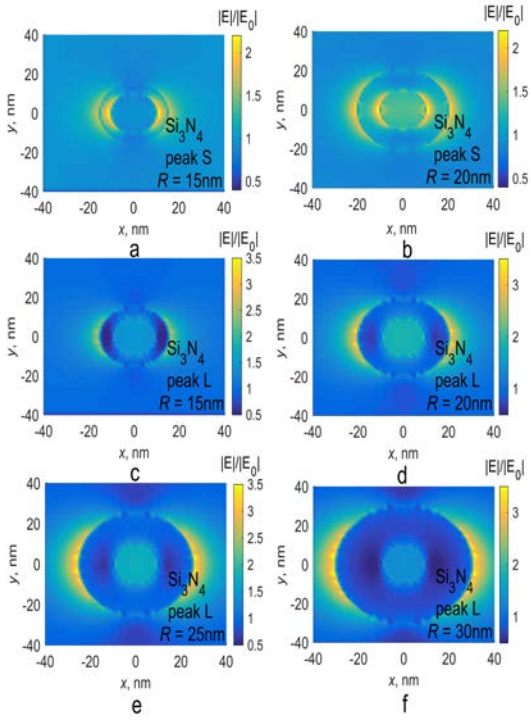

Fig. 4. Electric field distribution in the *x-y* plane for the case shown in Fig. 2 b. The nanoshell radius R: a, c – 15 nm; b, d – 20 nm; e – 25 nm; f – 30 nm. The wavelength correlates to a and b peak S, and c – f peak L. Note that the maximum intensity of the color bar is not the same

Comparing Fig. 4 a and b with Fig. 4 c and d, it is evident that for Si_3N_4 the electromagnetic modes that peaks S and L undergo are also different. In addition, the similarity between Fig. 4 c – f also illustrate that this plasmonic mode at the longer wavelength is associated with peak L. In this mode, the electric field appears mainly at the outer surface of the shell, and the electromagnetic 'hot spot' region becomes greater as the radius is increased.

Referring to Fig. 5 c, it is observed that for TiO_2 when the radius is large enough (R = 35 nm), the plasmonic resonance at about 240 nm gives rise to peak L. However, interestingly, the field distribution of the small radius (R = 15 nm), as indicated in Fig. 5 a, is observed to be different from that of R = 35 nm. Although there seems only one single peak in the scattering spectrum shown in Fig. 2 c, the field distribution results in Fig. 5 reveal that two plasmonic modes may overlap in the wavelength domain. It is dominated by the electromagnetic mode associated with peak L for the large radius, while once the radius is small enough the plasmonic mode of peak S takes over.

3.2. Fixed thickness of rhodium nanoshell

With a fixed thickness (i.e., $R - r$), the plasmonic properties of the rhodium nanoshell were also probed at the UV wavelengths, and the computed scattering spectra are given in Fig. 6. In the simulations the rhodium shell's thickness was always kept the same to be $R - r$ = 5 nm; this was achieved by varying the radius of the shell (R) and the radius of the core (r) simultaneously.

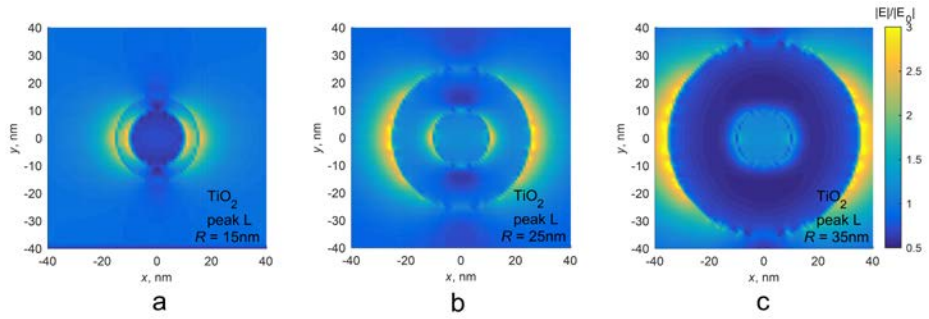

Fig. 5. Electric field distribution in the *x*-*y* plane for the case shown in Fig. 2 c. The nanoshell radius *R*: a – 15 nm; b – 25 nm; c – 35 nm. The wavelength correlates to the single peak

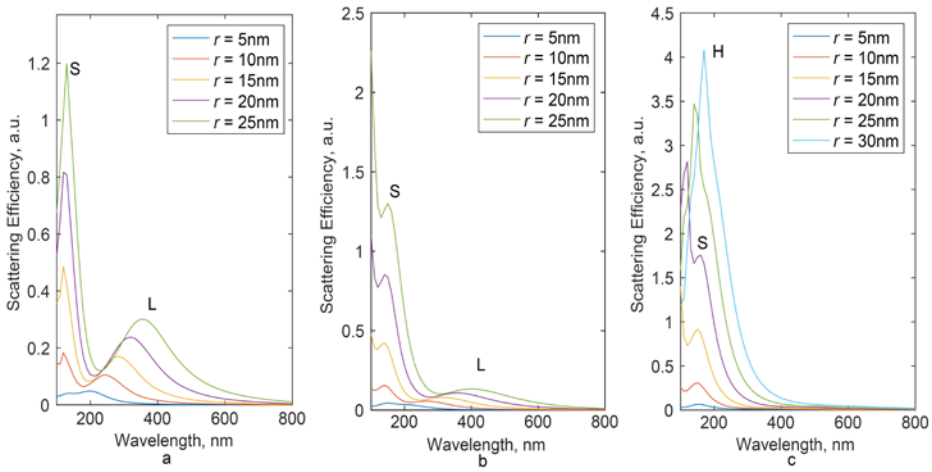

Fig. 6. Scattering efficiency as a function of incident light's wavelength. The dielectric material in the core: a – SiO_2; b – Si_3N_4; c – TiO_2. The thickness of the rhodium nanoshell was fixed to be $R - r = 5$ nm

Fig. 6a presents the results for the core being of SiO_2, and two peaks are observed in each scattering spectrum. It is clear that as the radii of *R* and *r* are decreased, the resonance wavelength for peak L is blueshifted from 360 to 200 nm, while peak S's wavelength shows few variations between 140 and 130 nm. Similar features are also witnessed in Fig. 6 b where the dielectric core was Si_3N_4. It is determined from Fig. 6 b that with reducing *r* from 25 to 5 nm, the resonance wavelength for peak L is blueshifted from 400 to 210 nm, whereas peak S has subtle changes around 140 nm. By comparing Fig. 6 a and b, the intensity of peak L of Si_3N_4 is much smaller than that of SiO_2.

Regarding Fig. 6 c, for the case of TiO_2 when the nanoshell is as small as $r = 20$ nm, two distinguishable peaks are observed. However, once the nanoshell is large (i.e., $r \geq 25$ nm) the resonance wavelengths of the two peaks become close, and the merge of the peaks results in a single-peak pattern in the scattering spectrum. As discussed above, it is necessary to attribute the peaks to different plasmonic modes by examining the electric field distributions. Therefore, the fields were further calculated and they are shown in Fig. 7 and Fig. 8.

By examining the field distributions in Fig. 7, it is found that the field patterns are all similar to the characteristic electromagnetic mode that is associated with peak S (referring to Fig. 4 a and b). In addition, for all the dielectric materials studied in this work, peak S undergoes a plasmonic resonance at the UV wavelengths between 120 and 160 nm. As the refractive index of the dielectric is increased from SiO_2 to TiO_2, the intensity of peak S is enhanced. With increasing the radius of the rhodium nanoshell, the peak's intensity is also increased.

From Fig. 8 a – e, it is clear that the electric fields of SiO_2 and Si_3N_4 at the resonance with a greater wavelength are characteristic to peak L. With reducing the radius of the nanoshell, this resonance has a substantial blueshift in the UV-Visible wavelength range from 400 to 200 nm. Referring to Fig. 8 c and f, interestingly, unlike SiO_2 and Si_3N_4, the TiO_2 possesses an additional electromagnetic mode that does not belong to either peak S or peak L. Known to the community, the surrounding dielectric may affect the plasmonic properties of noble metals. In this work, the presence of electric fields in the spatial region of the TiO_2 core, as shown in Fig. 8 c and f, unambiguously demonstrates the plasmonic mode that is associated with the effective coupling between the electron oscillations across TiO_2 and rhodium. Similar effects were also observed and addressed [26]. These effects illustrate that the local field enhancement on the surface of noble metal and resonance peak has a great relationship to the dielectric core. This electromagnetic mode is thus attributed to the peak that is labeled H in Fig. 6 c.

The key distinction between modes S, L, and H is that the electric field distributions are different, indicating various modes of electron oscillations. Referring to Fig. 8 a and b, it is shown that the electric field in mode L concentrates only on the rhodium nanoshell's surface, and there appear few effects by the core material. This indicates that mode L is to do with only the electron oscillation on the outer surface of the rhodium nanoshell.

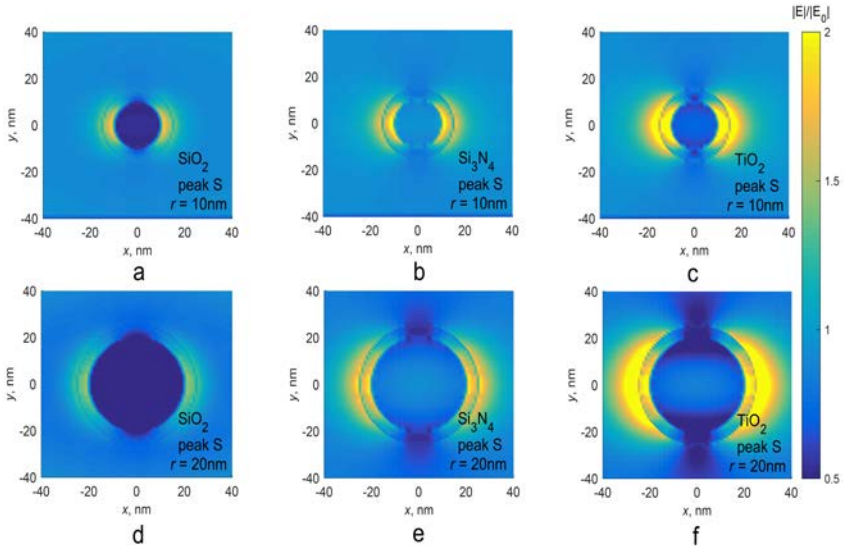

Fig. 7. Electric field distribution in the *x-y* plane for the case shown in Fig. 6. The dielectric core: a, d – SiO_2; b, e – Si_3N_4; e, f – TiO_2. The radius of the core: a, b, c – 10 nm; d, e, f – 20 nm. All the wavelengths correlate to peak S indicated in Fig. 6

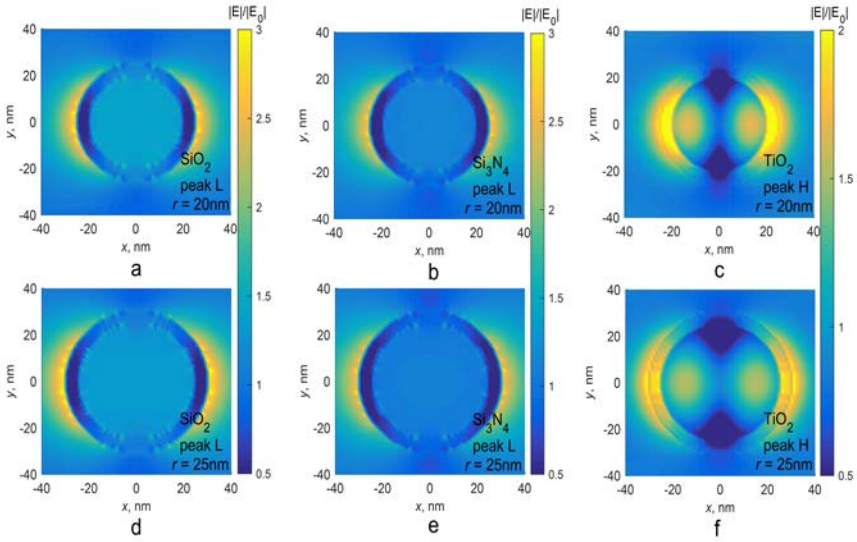

Fig. 8. Electric field distribution in the x-y plane for the case shown in Fig. 6. The dielectric core: a, d – SiO_2; b, e – Si_3N_4; c, f – TiO_2. The radius of the core: a, b, c – 20 nm; d, e, f – 25 nm. The wavelength correlates to a and d peak L in Fig. 6a; b and e peak L in Fig. 6 b; c and f peak H in Fig. 6 c. Note that the maximum intensity of the color bar is not the same

However, the field distributions for modes S (e.g., Fig.7c), and H (Fig.8c) are dramatically different from that of mode L. In mode S, the electrons oscillate not only on the outer surface of the nanoshell, but also at the interface between rhodium and the core dielectric material. In mode H, the electron oscillation appears both across rhodium and the core material.

4. CONCLUSIONS

In summary, the plasmonic properties of a nanoshell based optical nanomaterial consisting of a rhodium shell and dielectric core have been investigated. The scattering efficiency curves have been calculated in the wavelength range of 100 – 800 nm, with the FDTD method. Two resonance peaks have been witnessed in the UV regime, correlating to two different plasmonic modes, by examining the electric field distributions. The results have shown that the resonance wavelength of peak L is blueshifted as the nanoparticle radius is decreased from 35 to 25 nm, and meanwhile the peak intensity is increased. Based on this effect, the rhodium nanoshell-based nanomaterial may provide a promising platform for designing UV optical devices, whose plasmonic wavelength can be tuned by varying the size of the nanoparticle.

Acknowledgments

This work has been supported by the Basic Research Programme of Liaoning Province of China (LJKQZ2021171).

REFERENCES

1. **Ozbay, E.** Plasmonics: Merging Photonics and Electronics at Nanoscale Dimensions *Science* 311 2006: pp. 189 – 193. https://doi.org/10.1126/science.1114849

2. **Akimov, Y. A., Koh, W., Ostrikov, K.** Enhancement of Optical Absorption in Thin-Film Solar Cells Through the Excitation of Higherorder Nanoparticle Plasmon Modes *Optics Express* 17 (12) 2009: pp. 10195 – 10205. https://doi.org/10.1364/oe.17.010195
3. **Pillai, S., Catchpole, K., Trupke, T., Green, M.** Surface Plasmon Enhanced Silicon Solar Cells *Journal of Applied Physics* 101 2007: pp. 093105. https://doi.org/10.1063/1.2734885
4. **Barnes, W.L., Dereux, A., Ebbesen, T.W.** Surface Plasmon Subwavelength Optics *Nature* 424 2003: pp. 824 – 830. https://doi.org/10.1038/nature01937
5. **Kauranen, M., Zayats, A.V.** Nonlinear Plasmonics *Nature Photonics* 6 (11) 2012: pp. 737-748. https://doi.org/10.1038/NPHOTON.2012.244
6. **Yang, S.Z., Liu, Q.A., Liu, Y.L., Weng. G.J., Zhu, J., Li, J.J.** Recent Progress in the Optical Detection of Pathogenic Bacteria Based on Noble Metal Nanoparticles *Microchimica Acta* 188 2021: pp. 258. https://doi.org/10.1007/s00604-021-04885-z
7. **Farbod, M., Khademalrasool, M., Talebzadeh, M.D.** Plasmon-Enhanced Photocatalysis Based on Ag Plasmonic Nanospheres and ZnO Nanoparticles: Synthesis and Study Mechanisms Governing the Plasmonic Photocatalytic Performance *Plasmonics* 12 (3) 2017: pp. 759 – 769. https://doi.org/10.1007/s11468-016-0323-1
8. **Zhang, T.H., He, J.Y., Xie, W., Sun, C.** Plasmonic Properties of a Honeycomb Structure Formed by Metallic Nanoparticles *Physica E: Low-Dimensional Systems and Nanostructures* 118 2020: pp. 113901. https://doi.org/10.1016/j.physe.2019.113901
9. **Mott, D., Lee, J.D., Thi, N., Aoki, Y., Singh, P., Maenosono, S.** A Study on the Plasmonic Properties of Silver Core Gold Shell Nanoparticles: Optical Assessment of the Particle Structure *Japanese Journal of Applied Physics* 50 (6) 2011: pp. 065004. https://doi.org/10.1143/JJAP.50.065004
10. **Lv, J.W., Mu, H.W., Lu, X.L., Liu, Q., Liu, C., Sun, T., Chu, P.K.** Localized Surface Plasmon Resonance Properties of Symmetry-Broken Au-ITO-Ag Multilayered Nanoshells *Applied Physics A* 124 (6) 2018: pp. 437. https://doi.org/10.1007/s00339-018-1854-4
11. **Gashaw, B., Teshome, S., Belayneh, M.** Size Dependent Optical Properties of ZnO@Ag Core/Shell Nanostructures *Chinese Journal of Physics* 58 2019: pp. 235 – 243. https://doi.org/10.1016/j.cjph.2019.01.011
12. **Sun, C.** On the Plasmonic Properties of Ag@SiO2@Graphene Core-Shell Nanostructures *Plasmonics* 13 2018: pp. 1671 – 1680. https://doi.org/10.1007/s11468-017-0676-0
13. **Bhardwaj, S., Uma, R., Sharma, R.P.** A Study of Metal@Graphene Core-Shell Spherical Nano-Geometry to Enhance the SPR Tunability: Influence of Graphene Monolayer Shell Thickness *Plasmonics* 12 (4) 2017: pp. 961 – 969. https://doi.org/10.1007/s11468-016-0347-6
14. **Sekhon, J.S.** Facile Tuning and Refractive Index Sensitivity of Localized Surface Plasmon Resonance Inflection Points in Hollow Silver Nanoshells *Plasmonics* 16 (1) 2021: pp. 283 – 292. https://doi.org/10.1007/s11468-020-01277-6
15. **Khurana, K., Jaggi, N.** Localized Surface Plasmonic Properties of Au and Ag Nanoparticles for Sensors: A Review *Plasmonics* 16 2021: pp. 981 – 999. https://doi.org/10.1007/s11468-021-01381-1
16. **Kawachiya, Y., Murai, S., Saito, M., Sakamoto, H., Fujita, K., Tanaka, K.** Collective Plasmonic Modes Excited in Al Nanocylinder Arrays in the UV Spectral Region *Optics Express* 26 (5) 2018: pp. 5970 – 5982. https://doi.org/10.1364/OE.26.005970
17. **Gutierrez, Y., Alcaraz, D.L.O.R., Ortiz, D., Maria, S.J., Gonzalez, F., Moreno, F.** Plasmonics in the Ultraviolet with Aluminum, Gallium, Magnesium and Rhodium *Applied Sciences-Basel* 8 (1) 2018: pp. 64. https://doi.org/10.3390/app8010064
18. **Zhang, X., Li, P., Barreda, A., Gutierrez, Y., Gonzalez, F., Moreno, F., Everitt, H.O., Liu, J.** Size-Tunable Rhodium Nanostructures for Wavelength Tunable Ultraviolet Plasmonics *Nanoscale Horizons* 1 (1) 2016: pp. 75 – 80. https://doi.org/10.1039/c5nh00062a
19. **Ren, B., Lin, X.F., Yang, Z.L., Liu, G.K., Aroca, R.F., Mao, B.W., Tian, Z.Q.** Surface-Enhanced Raman Scattering in the Ultraviolet Spectral Region: UV-SERS on Rhodium and Ruthenium Electrodes *Journal of the American Chemical Society* 125 (32) 2003: pp. 9598 – 9599. https://doi.org/10.1021/ja035541d
20. **Watson, A.M., Zhang, X., Alcaraz, O.R., Marcos, S.J., Gonzlez, F., Moreno, F., Finkelstein, G., Liu, J., Everitt, H.O.** Rhodium Nanoparticles for Ultraviolet Plasmonics *Nano letters* 15 (2) 2015: pp. 1095 – 1100. https://doi.org/10.1021/nl5040623
21. **Ahmadivand, A., Sinha, R., Kaya, S., Nezih, P.** Rhodium Plasmonics for Deep-Ultraviolet Bio-Chemical Sensing *Plasmonics* 11 (3) 2016: pp. 839 – 849. https://doi.org/10.1007/s11468-015-0117-x
22. **Shiju, E., Abhijith, T., Rao, N.D., Chandrasekharan, K.** Nonlinear Optical Behavior of Au@Ag Core-Shell Nanostructures *Journal of Molecular Liquids* 333 2021: pp. 115935. https://doi.org/10.1016/j.molliq.2021.115935
23. FDTD Solutions, www.lumerical.com.
24. **Palik, E.D.** Handbook of Optical Constants of Solids *Academic Press* Vol. 3. 1998.
25. **Sun, C., Su, J., Wang, X.Q.** A Design of Thin Film Silicon Solar Cells Based on Silver Nanoparticle Arrays *Plasmonics* 10 2015: pp. 633 – 641. https://doi.org/10.1007/s11468-014-9849-2
26. **Li, Q., Zhang, Z.** Broadband Tunable and Double Dipole Surface Plasmon Resonance by TiO_2 Core/Ag Shell Nanoparticles *Plasmonics* 6 2011: pp. 779. https://doi.org/10.1007/s11468-011-9264-x